Lab on a Chip

Accepted Manuscript

ROYAL SOCIETY OF CHEMISTRY

www.rsc.org/loc

Cite this: DOI: 10.1039/c0xx00000x

www.rsc.org/xxxxxx

ARTICLE TYPE

Efficient single-cell poration by microsecond laser pulses

Qihui Fan,[a] Wenqi Hu[b] and Aaron T. Ohta*[b]

Received (in XXX, XXX) Xth XXXXXXXXX 20XX, Accepted Xth XXXXXXXXX 20XX
DOI: 10.1039/b000000x

Payloads including FITC-Dextran dye and plasmids were delivered into NIH/3T3 fibroblasts using microbubbles produced by microsecond laser pulses to induce pores in the cell membranes. Two different operational modes were used to achieve molecular delivery. Smaller molecules, such as the FITC-Dextran dye, were delivered via a scanning-laser mode. The poration efficiency and the cell viability were both 95.1 ± 3.0 %. Relatively larger GFP plasmids can be delivered efficiently via a fixed-laser mode, which is a more vigorous method that can create larger transient pores in the cell membrane. The transfection efficiency of 5.7-kb GFP plasmid DNA can reach to 86.7 ± 3.3 %. Using this cell poration system, targeted single cells can be porated with high resolution, and cells can be porated in arbitrary patterns.

Introduction

Molecular delivery is a fundamental application for biological research and some types of therapeutic treatments.[1] To achieve molecular delivery, cell poration techniques with high throughput, poration efficiency, and cell viability are desired, along with the ability to porate specific single cells with high resolution.

However, it is challenging to meet all of the previously mentioned requirements. Chemical- and viral- based transfection combines genetic material with different chemical or viral vectors, which will facilitate the transfer of genetic material into large groups of cells.[2, 3] Other bulk poration methods include electroporation, which uses pulsed electric fields to create transient pores in the cell membranes,[4] and sonoporation, which porates cells using acoustic energy facilitated by microbubbles.[5, 6] To porate specific single cells, a microcapillary or nanopipette handled by skilled operator is commonly used to serially inject molecules into single cells.[7, 8]

Optoporation is a promising technique for precise single-cell poration. It uses a laser to transiently increase the cell membrane permeability, and is an inherently non-contact, aseptic technique that also has the potential of parallel and automated operation. Femtosecond (fs) lasers can create submicrometer-sized pores in the membrane of targeted single cells by multi-photon processes and generation of a low-density plasma at the cell surface.[9-14] The transfection efficiency using femtosecond-laser poration can reach 80 to 90% for certain cell types,[12, 13] with a spatial resolution less than the size of a single cell.[9, 13, 14] However, to create these transient pores, the focal point of femtosecond laser needs to be precisely located on the cell membrane. This focus must be readjusted for each cell, as the poration efficiency drops by more than 50% for a mismatch of 3 μm between the laser focal plane and the cell membrane surface.[13] To improve the throughput, which is limited by serially adjusting the laser focus for each cell, various techniques were proposed, like the use of Bessel beams,[11, 13] or optically manipulated focusing lenses.[14]

Nanosecond (ns) lasers can also porate cells around laser-induced cavitation bubbles, but may result in heating and thermoelastic stresses on nearby cells.[13] In addition, the effective zone of nanosecond laser poration is too large for targeting single cells.[15] More precise control of ns-laser poration of individual cells is currently under study, with the goal of increasing efficiency and cell viability.[13, 16-19]

Continuous wave (CW) lasers can also be used for optoporation, achieved by heating the cell membrane to increase permeability. The cell viability after the poration process is high, but the transfection efficiency is less than 30%.[13, 20, 21]

There is room to explore between ns and CW lasers. Recently, lasers with microsecond pulse widths were also shown to be able to porate single cells, using a simple and economical setup.[22] In this laser-induced microbubble poration (LMP) system, a microbubble that oscillates in size was created by microsecond laser on an optically absorbent substrate near the edge of target cell.[22-27] The induced shear stress created transient pores in the cell membrane. This technique can achieve high poration efficiency (95.2 ± 4.8 %) while maintaining high cell viability (97.6 ± 2.4 %), although the throughput and the maximum deliverable molecular size still needs improvement.

This report describes further progress on poration using microsecond laser pulses. Unlike the previous LMP work,[22] the laser pulses creating the size-oscillating microbubbles were focused under the target cell, while maintaining a vertical separation between the bubble and cell. The shear stress induced by the oscillating bubble is highest above the microbubble center, facilitating poration within half a second per cell. Furthermore, there is limited lateral force, minimizing the possibility of dragging, damaging, or detaching the cells under poration. This poration method can maintain high poration efficiency and cell viability (both at 95.1 ± 3.0 %), and has sufficient spatial resolution to porate single cells. The poration method described

in this paper can also provide a much higher throughput as compared to previous LMP results.[22] Previously, each cell took 15 s per poration operation; in the new system, this duration has been reduced to 0.4 s per cell. Moreover, since the shear stress produced by the bubble is stronger compared to previously demonstrated LMP results,[22] this technique can create larger pores for the delivery of larger molecules.[28]

Materials and methods

Setup for poration system

The microsecond laser pulse was produced by a 980-nm diode laser (Laserlands, 980MD-0.8W-BL) and focused on the bottom of a fluidic chamber from beneath, in which the cells were porated (Fig. 1). The laser with a maximum power of 800 mW was controlled by a function generator (Agilent 33220A) to generate and modulate on and off pulse cycles via a TTL pulse signal. A 20X objective lens was mounted in front of the laser to focus the laser to a 4.4 μm-diameter spot, corresponding to a measured intensity of 508 kW/cm^2. The laser was settled on an X-Y stage, which can be controlled to move at certain speeds by a motion controller (Newport MM3000).

The fluidic chamber for cell poration is formed by clamping an optically absorbent substrate and a glass slide together. The bottom optically absorbent substrate is a 1-mm-thick glass slide, deposited with a layer of indium tin oxide (ITO) with 200 nm thickness, and subsequently with another layer of amorphous silicon (α-silicon) with 1 μm thickness. Around 70 % of the incident light from laser was absorbed by this substrate and then converted into heat,[29] which induced the vapour microbubbles in the fluidic chamber at the position of the laser spot on the substrate. A cell monolayer was pre-cultured on the glass slide which was for the top of the chamber, and the cell monolayer was faced towards the interior of the chamber. Uniform-sized polystyrene beads (Polysciences, Inc.) functioned as spacers for the chamber, allowing discrete adjustment of the chamber height. Spacers were put on two opposite sides of the chamber, and the other two sides were left open for the fluid exchange.

The bubble position can be adjusted by controlling the laser position via the motion controller to interact with the target cells. The poration duration, or the time of the bubble-cell interaction, can be regulated for each cell using two modes. The first mode (scanning-laser mode) scans the laser at a constant velocity along a path that intersects the cell position. The laser can start at any point near the target cell, as long as the laser path intersects the cell location. The laser scans the cells at a uniform velocity and creates pores along the path regardless of the orientation of the scanning path with respect to the cell. Typically, the laser path is orthogonal to the long axis of the cell. Since only the scanning velocity is controlled, scanning over a larger cell will result in a greater bubble-cell interaction time, although the deviation in interaction time is minimal for the homogeneous cell population used in the experiments presented here. This mode fixes the bubble-cell interaction time per cell, but also prevents the laser and bubble from remaining at a fixed point on the cell membrane. This scanning mode is suitable for rapidly porating cells in arbitrary patterns. The second mode (fixed-laser mode) fixes the laser in a certain position; the exposure time of the laser pulses is then set to achieve a controllable bubble-cell interaction time. The laser pulses repeat at a rate of 50 Hz. By focusing the laser on one point on the cell membrane, larger pores can be produced. This mode is more functional for the delivery of larger molecules, and for more precise single-cell poration.

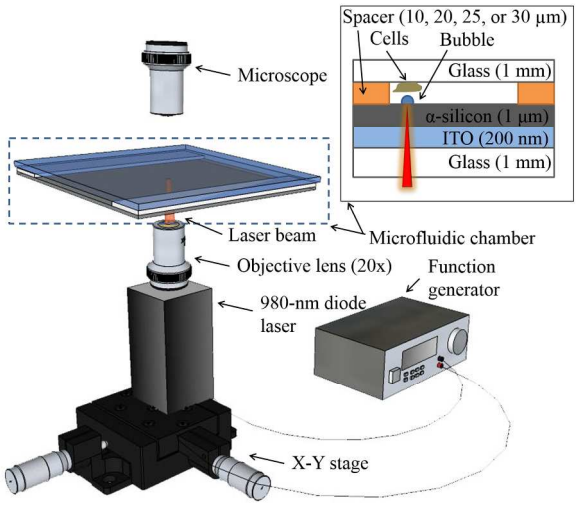

Fig. 1 Setup for the cell poration system using microsecond laser-induced oscillating microbubbles. A 980-nm diode laser was modulated by a function generator and focused onto an optically absorbent substrate, creating microbubbles that oscillated in size in the microfluidic chamber. The inset shows the structure of the microfluidic chamber, which consists of a glass slide coated with 200-nm indium tin oxide (ITO) and 1-μm amorphous silicon (α-silicon) layers, and a chamber ceiling made of a glass slide with cultured cells.

Cell culture

NIH/3T3 fibroblasts (ATCC) were grown in Dulbecco's Modified Eagle's Medium (DMEM, ATCC), with 10 % bovine serum (Gibco, Invitrogen), penicillin (100 U/ml), and streptomycin (100 μg/ml), at 37 °C in 5 % CO_2. The cells were cultured on sterile glass slides to 50 to 70 % confluency before testing.

Cell poration and transfection

Fluorescein-isothiocyanate-(FITC) conjugated Dextran (Sigma-Aldrich, MW = 3 kDa, 70 kDa, 150 kDa, and 500 kDa), and 5.7-kb green fluorescent protein (GFP) plasmid DNA (Invitrogen) were used as demonstration molecules for delivery. One day prior to testing, 3T3 cells were pre-cultured on a sterilized glass slide (25 mm × 10 mm). Immediately before the poration procedure, the glass slide with the attached 3T3 cells was removed from the culture medium and washed with phosphate-buffered saline (PBS) to remove debris. The glass slide is used as the ceiling of the fluidic chamber, with the cell monolayer facing towards the chamber interior. A solution of 15 mg/ml FITC-Dextran in 1X PBS or 33 ng/μl GFP plasmid DNA in DMEM with 10 % bovine serum was prepared and added to the fluidic chamber for the molecular delivery. The interaction of the microbubbles and the

target cells resulted in poration of specific cells. After molecules were delivered, the excess FITC-Dextran or GFP plasmid DNA was rinsed thoroughly with cell culture medium without antibiotics. Poration was verified by observing cells with green fluorescence from FITC or GFP under an epi-fluorescent microscope. The camera settings, such as exposure time and gain value, were kept constant over the various experiments. The recorded images were analysed using ImageJ software. Cells were recorded as successfully porated if the green colour intensity values were higher than 50, on a scale of 0 to 255, and if the cells were verified as viable in a subsequent cell viability test. Thus, the poration efficiency, defined here as the percentage of cells with successful molecular delivery, never exceeds the percentage of viable cells.

Cell viability assay

Propidium iodide (PI, Invitrogen), a membrane-impermeable fluorescent dye, was used to assess the cell viability. PI can only enter cells with damaged membranes; it then binds to nucleic acids to emit a red fluorescence, indicating dead cells. Approximately 5 to 20 minutes after cell poration, 50 µg/ml PI in DMEM with 10 % bovine serum was loaded into the fluidic chamber and incubated with cells for 5 to 20 minutes. Cells were then imaged under an epi-fluorescent microscope to observe PI fluorescence, testing cell viability.

Mechanism and characterization

Mechanism

The mechanism of creating pores in cell membrane is illustrated in Fig. 2. The microsecond-laser pulses induced microbubbles that oscillate in size. The rapid bubble expansion cycles cause the microstreaming around microbubble.[30, 31]

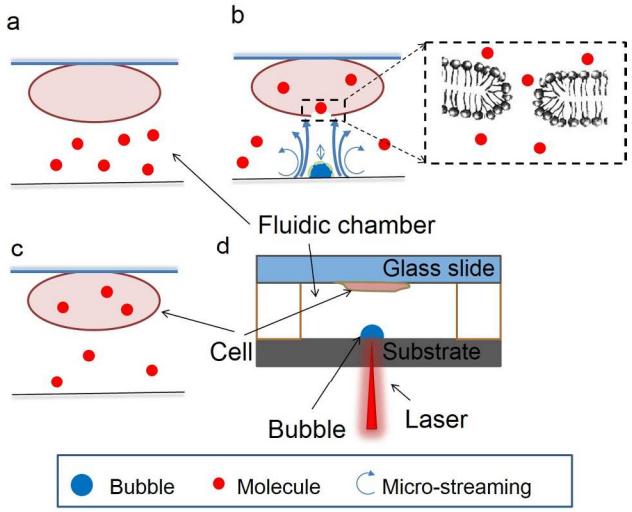

Fig. 2 The mechanics of cell poration by laser-induced microbubbles. (a) Initially, the cell membrane is impermeable to large molecules outside the cell. (b) A microbubble that oscillates in size is induced on a surface directly below the target cell. Microstreaming flow surrounding the bubble opens transient pores in the cell membrane, as shown in the inset, allowing molecules to enter the cell. (c) When the laser pulses cease, the microbubble dissolves rapidly and the cell membrane reseals, completing the cell poration process. (d) The cell and microbubble positions shown in the context of the fluidic chamber used in the poration system.

The dynamic bubble diameter was measured to quantify the size oscillation (Fig. 3). A laser pulse width of 60 µs is the minimum value for the formation of oscillating bubbles. The bubbles created by the 60-µs pulse have a size oscillation range (the difference between maximum and minimum bubble diameter) of 2.1 µm. The 80-µs pulse width induced bubbles in a size oscillation range of 2.4 µm. The 100-µs pulse width created significantly larger bubbles that also had a greater size oscillation range (3.2 µm), which corresponds to larger shear stress. The diameter of the bubbles induced by the 140-µs laser pulse is dramatically larger than the other pulse widths, but the bubble size is nearly constant, indicating weak microstreaming and associated shear stress.

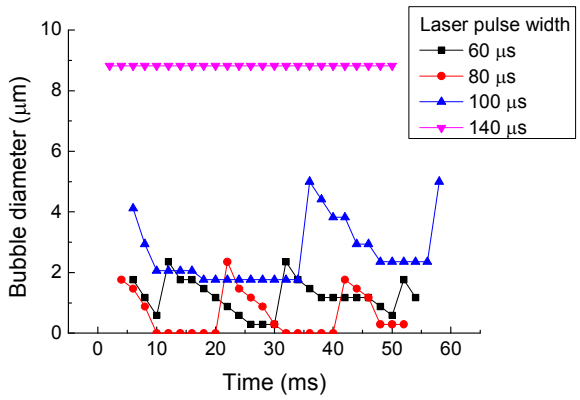

Fig. 3 Measured dynamic bubble diameter for laser pulse widths of 60, 80, 100, and 140 µs.

The microstreaming surrounding the bubbles has been visualized with tracer particles (0.5-µm-diameter polystyrene beads), as shown in Fig. S2 in the electronic supplementary information (ESI) accompanying this article. The microstreaming reaches its highest speed in vertical direction above the center of the bubble,[30, 32] so a cell right above the bubble experiences the strongest effective shear stress for creating pores in membrane. The tracer bead velocity in the vertical direction of microstreaming is at least 898 µm/s above the center of the bubble, while the bead horizontal velocity is generally within the range of 200 µm/s (Fig. S3 in the ESI). It is estimated that the resultant shear stress at the membrane of a cell under poration is on the order of the critical stress needed for cell poration, 3 kPa.[31, 33] Porating the cell right above the bubble also corresponds to the point with the lowest lateral shear force, reducing the likelihood of cell detachment from the surface. Shear stress on the cell membrane can be modulated by adjusting the chamber height and other parameters.

The molecules in the fluidic chamber are membrane impermeable (Fig. 2a). The laser pulses induce a size-oscillating bubble under the target cell, and the shear stress around the microbubble opens small transient pores in cell membrane (Fig. 2b). Poration occurs for a set duration, then the laser pulses cease,

and the microbubble dissolves into the solution rapidly. The cell membrane reseals, completing the molecular delivery (Fig 2c).

Since the laser is directly incident upon the cells, a test to check for cell poration and cell viability was conducted in the presence of laser light, but without microbubbles. The results are shown in the ESI. Briefly, a clear glass slide was used as the bottom of the fluidic chamber, replacing the optically absorbent substrate. All other procedures were the same as in the cell poration and cell viability tests described in the previous section. In this setup, much more light reaches the cell under poration; nonetheless, the targeted cells did not show any red fluorescence, indicating the cells were not damaged by the laser (Fig. S1 in ESI). The cells also did not display any green fluorescence, indicating that poration does not occur if cells are merely exposed to laser with no microbubbles present.

Scanning-laser mode

The 3-kDa FITC-conjugated Dextran was used as demonstration molecules for the characterization tests of scanning-laser mode. Various laser pulse widths can influence the bubble oscillating strength and the corresponding shear stress to the target cells. The microbubble formation and the induced microstreaming occurs when the laser pulse width was at least 60 µs, so this is the minimum pulse width used for cell poration. This pulse width can induce sufficient shear stress for effective cell poration, while minimizing cellular damage, as both the poration efficiency and the cell viability are 95.1 ± 3.0 % (Fig. 4). If the pulse width was increased to 80 or 100 µs, the shear stress induced by microstreaming was stronger and caused more damage to the nearby cells, as indicated by the lower cell viability and the corresponding limited poration efficiency (both around 80.0 %). Further increasing the pulse width to 140 µs results in a larger microbubble and a smaller bubble size oscillation, as shown in Fig. 3, which is similar to the bubble behaviour previously reported.[22] This induces less shear stress around target cells, lowering the cell poration efficiency to 33.3 ± 14.5 %, while maintaining a high cell viability of 93.3 ± 3.3 %. The viability of the sample group of cells prior to the poration was not tested, since the PI test is destructive; however, the viability of the cell cultures was approximately 100 %, meaning that any significant drop in viability is likely from the poration process.

Two parameters other than laser pulse width were also characterized to find the optimal cell poration performance. A laser scanning speed of 50 µm/s and a fluidic chamber height of 20 µm were determined as the optimal conditions. The results are in the ESI (Fig. S4 and S5).

Fixed-laser mode

This operating mode is more suited for delivery of larger molecules; thus, 5.7-kb GFP plasmids were used as demonstration molecules for the characterization tests of this mode. In this fixed-laser mode, the shear stress from the microbubble is applied repeatedly on one point of the cell, producing larger pores in cell membrane, and allowing the delivery of larger molecules.

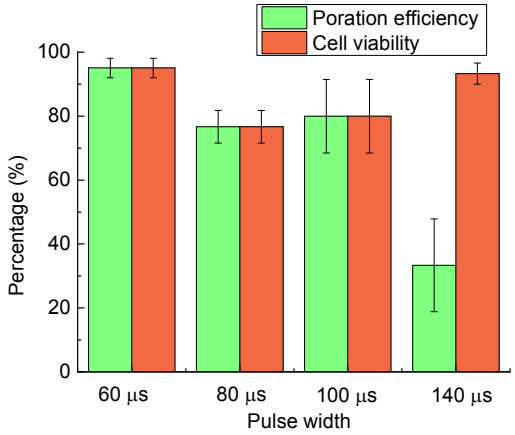

Fig. 4 Cell poration efficiency and cell viability as a function of the pulse width in the scanning-laser mode. Error bars show the standard error of the measurements. More than 30 cells were tested in three parallel experiments for each pulse width.

The previous characterization results for the scanning-laser mode showed that chamber heights of 10 µm and 20 µm can both provide acceptable poration efficiency, along with laser pulse widths of 60 µs and 100 µs. Thus, these two pulse widths were tested in the fixed-laser mode using 10- and 20-µm chamber heights. An important parameter for the fixed-laser mode is poration duration, or the amount of time that the cell is subjected to the microbubble poration. This was varied from 100 ms to 600 ms. For a chamber height of 10 µm, the transfection efficiency using a 60-µs laser pulse width of 400 ms duration is 86.7 ± 3.3 % (Fig. 5a). The transfection efficiency using a 100-µs pulse width with the same duration is lowered to 30.0 ± 25.2 %, since the microstreaming from the oscillating bubble induced under these conditions may be too vigorous to maintain cell viability. The transfection efficiency is highest when the poration duration is 400 ms. Poration durations greater than 400 ms can increase the chances of cell poration, but may also cause more cell damage, while poration durations shorter than 400 ms do not provide as high a transfection efficiency. Thus, a 400-ms poration duration was selected as a compromise. For a 20-µm chamber height, the working distance between the oscillating bubble and cell membrane is too great for efficient transfection, especially when using the 60-µs laser pulse (Fig. 5b). When using a 100-µs laser pulse width, the transfection efficiency is 60.0 ± 20.0 % for a 200-ms duration. This is higher than the efficiency for these conditions at a 10-µm chamber height, since the longer distance between the bubble and cell membrane decreases damage to the cell.

The optimized parameters from the previous characterization tests for both the scanning-laser mode and fixed-laser mode are summarized in Table 1. These parameters were used in the following experiments as the optimized conditions for each mode.

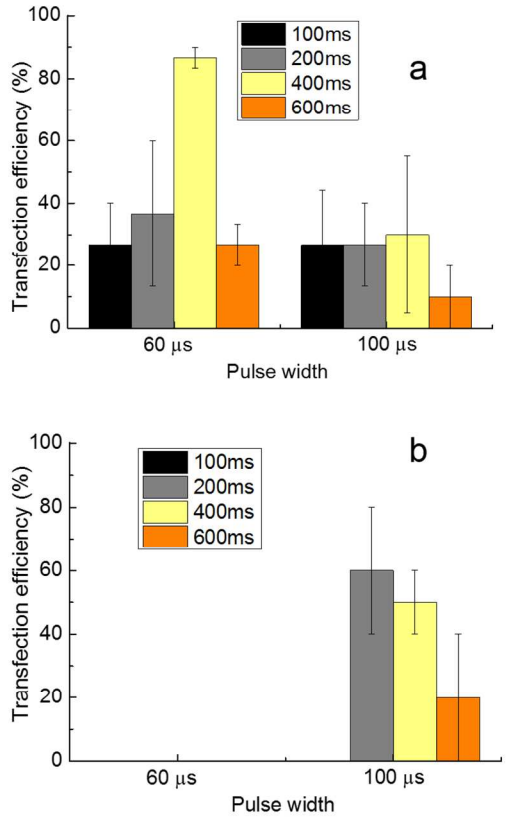

Fig. 5 Cell transfection efficiencies for various poration durations as a function of the pulse width, using 10- and 20-μm chamber heights in the fixed-laser mode. (a) 10 μm chamber height. (b) 20 μm chamber height. Error bars show the standard error of the measurements. More than 30 cells in (a) and 15 cells in (b) were tested for each condition.

Table 1 Optimized poration conditions.

Characterization items	Scanning mode	Fixed mode
Pulse width	60 μs	60 μs
Laser scanning speed	50 μm/s	N/A
Chamber height	20 μm	10 μm
Poration duration	N/A	400 ms

Size of transient pores in cell membrane

The size of FITC-Dextran can be controlled by varying the molecular weight of the conjugated polymer Dextran. Four different sizes of FITC-Dextran were chosen to test the molecular size capacity, determined by the induced transient pore size. The molecular weights of these FITC-Dextran are 3 kDa, 70 kDa, 150 kDa, and 500 kDa, individually, with the approximate Stoke's diameters of 2.8 nm, 12 nm, 17 nm, and 29.4 nm, respectively. The cell poration result is shown in Fig. 6. The poration efficiency in the scanning-laser mode can reach to 95.1 ± 3.0 % for 3-kDa FITC-Dextran, and then gradually decreases to 82.2 ± 9.7 % for 70-kDa FITC-Dextran, 42.2 ± 21.2 % for 150-kDa FITC-Dextran, and finally 27.5 ± 11.1 % for 500-kDa molecules, while the cell viability can reach 100 %. The poration efficiency is acceptable up to the 500-kDa size, suggesting that the induced pore size is at least 30 nm. The poration efficiencies of 150-kDa and 500-kDa FITC-Dextran are higher than previous results using the LMP method,[22] indicating that this scanning-laser mode is not only faster than LMP, but also creates larger transient pores to improve the poration efficiency.

The fixed-laser mode can create even larger transient pores, indicated by the cell poration result of 500-kDa FITC-Dextran in fixed-laser mode. Under the optimized parameters, the poration efficiency for 500-kDa FITC-Dextran in the fixed-laser mode can reach to 70.0 ± 10.0 %, while the corresponding cell viability is approximately 90 %.[28]

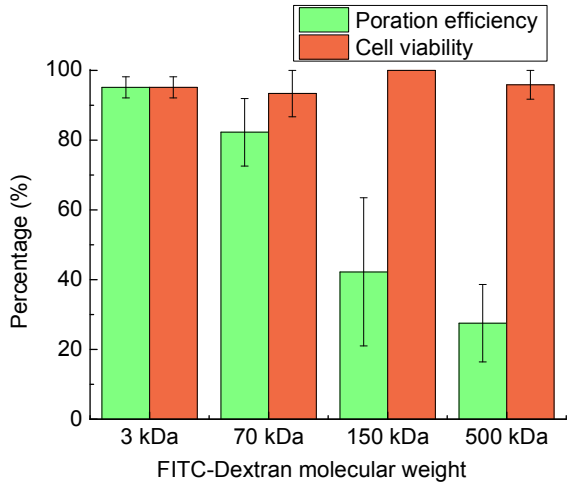

Fig. 6 Cell poration efficiency and cell viability in the scanning-laser mode for FITC-Dextran molecules of various sizes (3 kDa, 70 kDa, 150 kDa, and 500 kDa). More than 30 cells were tested in three parallel tests for each molecular size. Note that all cells in the 150-kDa group were viable following poration, thus there is no standard error for this column.

Results and discussion

Targeted cell poration

As the characterization results show, the efficiency of 3-kDa FITC-Dextran molecular delivery via the scanning-laser mode can reach to 95.1 ± 3.0 %, with a similar cell viability. A demonstration of this is the poration of five randomly selected cells in a field of view (Fig. 7). Laser-induced microbubbles were scanned over each cell, porating five target cells as indicated by the green fluorescence from 3-kDa FITC-Dextran dye. No red fluorescence was observed, indicating the cells are viable. It took 70 s to locate and porate all five cells, although this time can be reduce further by automated operation, since it takes approximately 500 ms to porate each cell at the optimal laser scanning speed.

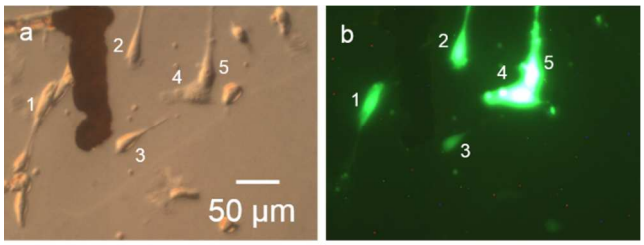

Fig. 7 Successful molecular delivery to five targeted NIH/3T3 fibroblasts using the scanning-laser mode. (a) Numerically labelled porated cells. (b) All target cells display only green fluorescence, indicating that all cells were successfully porated with 3-kDa FITC-Dextran dye. The absence of red fluorescence from PI indicates the cells are viable.

Single-cell poration/transfection

Targeted single cells can be porated or transfected precisely without affecting neighbouring cells, in both the scanning-laser mode and the fixed-laser mode. As shown in Fig. 8 and Fig. 9, only the targeted single cells displayed green fluorescence from FITC or GFP, indicating successful precise molecular delivery.

After the cell poration, cell viability tests were conducted immediately to test for cell membrane damage. Subsequently, cells were cultured and observed for a few days to check cell activity and proliferation. After the cells were porated in the fluidic chamber, the glass slide with the cell monolayer was carefully detached while immersing the whole fluidic chamber in 1X PBS buffer. The immersion helps to avoid cell damage by the air-water meniscus when the fluidic chamber is separated. The cell monolayer sample was put into fresh complete cell culture medium in a sterile petri dish, and cultured in an incubator. The position of the targeted cells was registered to the marks on the substrate so that the same cells can be observed each day.

Using the scanning-laser mode, one target cell was porated with 3-kDa FITC-Dextran under the optimal conditions. As shown in Fig. 8, the bright green fluorescence in the targeted cell shows the successful molecular delivery immediately after the poration procedure. One day after poration, the cell has spread and adhered onto the substrate. The cell divided on second day, and again on the third day after poration. The green fluorescent intensity from the FITC-Dextran in the cell kept decreasing as it was distributed to multiple cells during cell division.

Using the fixed-laser mode, 5.7-kb GFP plasmids were transfected. After 12 to 24 hours, GFP was expressed in the transfected cell, and the cell exhibits green fluorescence (Fig. 9). On the second day of culture, the cell has proliferated normally.

Patterned delivery of multiple payloads

The scanning-laser mode can also porate cells in arbitrary patterns. Moreover, since the solution containing the molecules can be replaced easily in the fluidic chamber, two or more kinds of molecules can be delivered into the same cell sample, as desired. This delivery of multiple molecules can enable potential applications like the differentiation of neighbouring stem cells to various specialized cell types required for the formation of a tissue or organ.

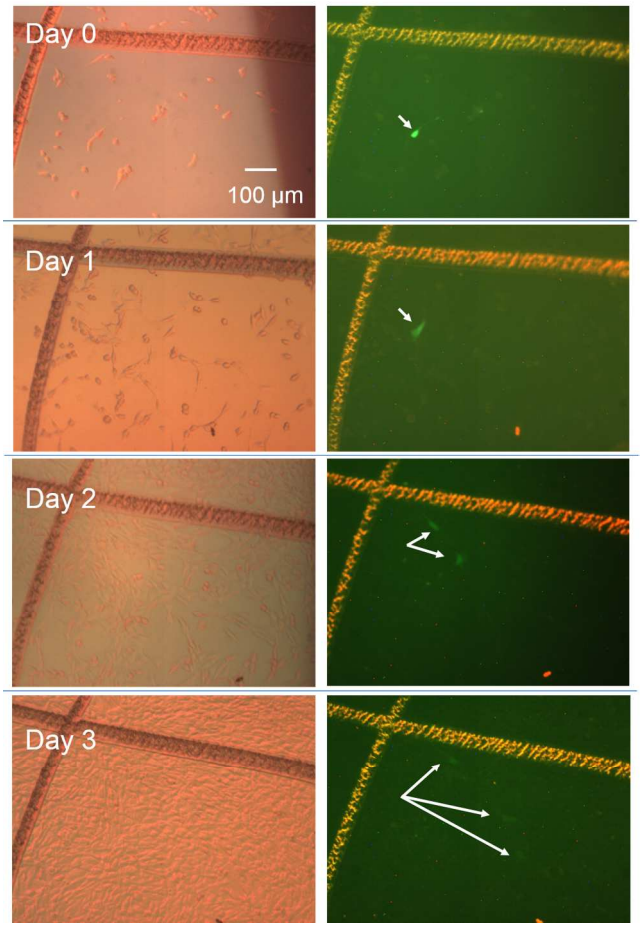

Fig. 8 Single-cell poration for the delivery of 3-kDa FITC-Dextran using the scanning-laser mode. The left column of images shows the brightfield images of the porated cell, while the right column shows the corresponding fluorescent images. The porated cell and its visible daughter cells are marked by arrows. Images were taken each day starting with the day of successful cell poration (Day 0) to the third day of cell culture. The cell exhibits bright green fluorescence from delivered FITC-Dextran on Day 0 and Day 1. The cell divided on Day 2 and keeps proliferating through Day 3.

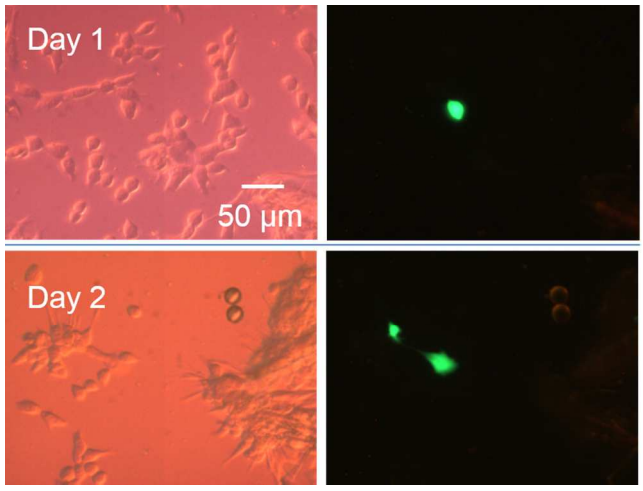

Fig. 9 Single-cell transfection using the fixed-laser mode. The left column of images shows the brightfield images of the transfected cell, while the right column shows the corresponding fluorescent images. The images were taken on the first and second days following the transfection

operation. The GFP was expressed from Day 1 after the transfection, and the cell proliferated normally on Day 2.

This concept was demonstrated using two molecules: 3-kDa FITC-Dextran and PI. First, the 3-kDa FITC-Dextran was delivered into the cells positioned along the trajectory of the scanning laser. Then, the FITC-Dextran solution was replaced by PI solution by using a piece of filter paper to wick away the FITC-Dextran solution from the side of the fluidic chamber while simultaneously introducing the PI solution by capillary action. The cell poration was then conducted again to deliver the PI into different cells. The result of the patterned delivery of the two molecules is shown in Fig. 10. The upper dashed line marks the laser scanning path for the FITC-Dextran, and the lower dashed line corresponds to the laser scanning path for the PI delivery (Fig 10a). A composite fluorescent image shows the successful delivery of the green FITC-Dextran and red PI (Fig. 10b). It took 8 s per type of molecule to porate the cells.

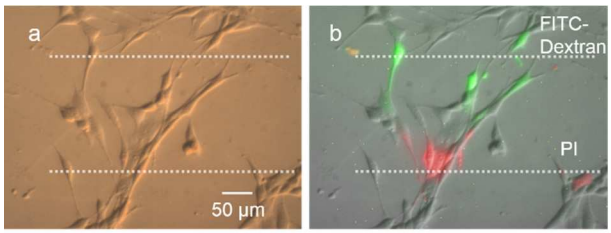

Fig. 10 Patterned delivery of multiple payloads. 3-kDa FITC-Dextran was delivered into the cells along the pattern marked by the upper dashed line, while PI was delivered into cells along the pattern marked by the lowered dashed line. (a) Brightfield image of the porated cells. (b) Composite fluorescent image shows the successful delivery of both FITC-Dextran (green fluorescence) and PI (red fluorescence).

Conclusions

Localized single-cell poration by microsecond-laser-pulse-induced microbubbles was demonstrated and characterized. The laser-induced bubble is able to porate targeted single cells with high poration efficiency and cell viability. This system provides a simple and economical method for efficient targeted single-cell poration, and has higher throughput than previously reported LMP method.[22] The microsecond-laser-induced microbubble poration method inherits the advantages of other optoporation methods, including the targeting of specific spatial locations. This microsecond laser system complements existing optoporation methods by improving upon the 30% poration efficiency of CW-laser poration, increasing spatial resolution as compared to ns-laser poration, and using a simpler and more affordable hardware setup compared to fs-laser poration systems. The microsecond-laser-induced cell poration method can achieve a poration efficiency of up to 95.1 ± 3.0 % for 3-kDa FITC-Dextran using the scanning-laser mode. Larger 5.7-kb GFP plasmids can be transfected at up to 86.7 ± 3.3 % efficiency using the fixed-laser mode. The test result of molecules with sizes varying from 2.8 nm to 29.4 nm in the scanning-laser mode, and the relatively high poration efficiency of 70.0 ± 10.0 % for 500-kDa FITC-Dextran[28] in the fixed-laser mode both suggest that the average induced pore size is over 30 nm, showing an increased capability for delivery of larger molecules as compared to previous LMP results.[22] The induced pore size in this method is similar to the size range achievable by sonoporation and electroporation.[34, 35] Larger pore sizes can be achieved by other poration methods: up to 200 nm by chemical poration,[36] more than 20 μm by microinjection,[37] and 1 μm by fs-laser poration.[14]

Both the scanning-laser mode and fixed-laser mode can selectively porate single cells in specific spatial locations. Subsequent cell culture after poration shows normal cell proliferation. The rapid delivery of multiple types of molecules into the same cell monolayer sample is also a feature with many potential important applications. In addition, if multiple macromolecules are to be delivered into same cell, this can be done in a single operation by mixing the various molecules before the cell poration.

In the future, the parallel control of microbubbles will be developed, enabling the poration of multiple target cells at the same time. This will increase the throughput of the system, which is currently around 400 ms per cell. A spatial light modulator or scanning mirror system can be integrated for the parallel and automated control of the cell poration. These systems can project a single laser onto multiple areas of the substrate within one period, and the multiple laser spots can also be automatically controlled by software.

Acknowledgement

This project was supported in part by Grant Number 1R01EB016458-01 from the National Institute of Biomedical Imaging and Bioengineering of the National Institutes of Health (NIH) as part of the NSF/NASA/NIH/USDA National Robotics Initiative. These contents are solely the responsibility of the authors and do not necessarily represent the official views of the NIH.

Notes

[a] *Department of Mechanical Engineering, University of Hawaii at Manoa, 2540 Dole Street, Holmes Hall 302, Honolulu, USA. Fax: +1-808-956-3427; Tel: 808-956-3427; E-mail: fanqihui@hawaii.edu*
[b] *Department of Electrical Engineering, University of Hawaii at Manoa, 2540 Dole Street, Holmes Hall 483, Honolulu, USA. E-mail: wenqihu@hawaii.edu, aohta@hawaii.edu*
† Electronic Supplementary Information (ESI) available: [details of any supplementary information available should be included here]. See DOI: 10.1039/b000000x/

References

1. S. Lakshmanan, G. K. Gupta, P. Avci, R. Chandran, M. Sadasivam, A. E. Jorge and M. R. Hamblin, *Adv Drug Deliv Rev*, 2014, **71**, 98-114.
2. P. Midoux, C. Pichon, J.-J. Yaouanc and P.-A. Jaffrès, *British Journal of Pharmacology*, 2009, **157**, 166-178.

3. J. Wang, S. M. Faust and J. E. Rabinowitz, *Journal of Molecular and Cellular Cardiology*, 2011, **50**, 793-802.
4. A. M. Bodles-Brakhop, R. Heller and R. Draghia-Akli, *Molecular Therapy*, 2009, **17**, 585-592.
5. S. Mitragotri, *Nature Reviews Drug Discovery*, 2005, **4**, 6.
6. Y. Qiu, C. Zhang, J. Tu and D. Zhang, *Journal of Biomechanics*, 2012, **45**, 1339-1345.
7. Y. Zhang, *Nat Protoc*, 2007, DOI: 10.1038/nprot.2007.1487.
8. S.-W. Han, C. Nakamura, N. Kotobuki, I. Obataya, H. Ohgushi, T. Nagamune and J. Miyake, *Nanomedicine: Nanotechnology, Biology and Medicine*, 2008, **4**, 215-225.
9. U. K. Tirlapur and K. Konig, *Nature*, 2002, **418**, 290-291.
10. D. Stevenson, B. Agate, X. Tsampoula, P. Fischer, C. T. Brown, W. Sibbett, A. Riches, F. Gunn-Moore and K. Dholakia, *Opt Express*, 2006, **14**, 7125-7133.
11. X. Tsampoula, V. Garces-Chavez, M. Comrie, D. J. Stevenson, B. Agate, C. T. A. Brown, F. Gunn-Moore and K. Dholakia, *Appl Phys Lett*, 2007, **91**, 053902-053902-053903.
12. A. Uchugonova, K. Konig, R. Bueckle, A. Isemann and G. Tempea, *Opt Express*, 2008, **16**, 9357-9364.
13. D. J. Stevenson, F. J. Gunn-Moore, P. Campbell and K. Dholakia, *Journal of the Royal Society, Interface / the Royal Society*, 2010, **7**, 863-871.
14. M. Waleed, S.-U. Hwang, J.-D. Kim, I. Shabbir, S.-M. Shin and Y.-G. Lee, *Biomed. Opt. Express*, 2013, **4**, 1533-1547.
15. R. Dijkink, S. Le Gac, E. Nijhuis, A. van den Berg, I. Vermes, A. Poot and C. D. Ohl, *Phys Med Biol*, 2008, **53**, 375-390.
16. S. Le Gac, E. Zwaan, A. van den Berg and C. D. Ohl, *Lab Chip*, 2007, **7**, 1666-1672.
17. G. N. Sankin, F. Yuan and P. Zhong, *Physical Review Letters*, 2010, **105**, 078101.
18. C. T. Hsiao, J. K. Choi, S. Singh, G. L. Chahine, T. A. Hay, Y. A. Ilinskii, E. A. Zabolotskaya, M. F. Hamilton, G. Sankin, F. Yuan and P. Zhong, *J Fluid Mech*, 2013, **716**.
19. Z. G. Li, A. Q. Liu, E. Klaseboer, J. B. Zhang and C. D. Ohl, *Lab Chip*, 2013, **13**, 1144-1150.
20. H. Schneckenburger, A. Hendinger, R. Sailer, W. S. Strauss and M. Schmitt, *J Biomed Opt*, 2002, **7**, 410-416.
21. A. V. Nikolskaya, V. P. Nikolski and I. R. Efimov, *Cell communication & adhesion*, 2006, **13**, 217-222.
22. Q. Fan, W. Hu and A. T. Ohta, *Lab Chip*, 2014, **14**, 1572-1578.
23. S. Fujii, K. Kanaizuka, S. Toyabe, K. Kobayashi, E. Muneyuki and M.-a. Haga, *Langmuir*, 2011, **27**, 8605-8610.
24. K. Zhang, A. Jian, X. Zhang, Y. Wang, Z. Li and H.-y. Tam, *Lab Chip*, 2011, **11**, 1389-1395.
25. Y. Zheng, H. Liu, Y. Wang, C. Zhu, S. Wang, J. Cao and S. Zhu, *Lab Chip*, 2011, **11**, 3816-3820.
26. Y. Xie, C. Zhao, Y. Zhao, S. Li, J. Rufo, S. Yang, F. Guo and T. J. Huang, *Lab Chip*, 2013, **13**, 1772-1779.
27. C. Zhao, Y. Xie, Z. Mao, Y. Zhao, J. Rufo, S. Yang, F. Guo, J. D. Mai and T. J. Huang, *Lab Chip*, 2014, **14**, 384-391.
28. Q. Fan, W. Hu and A. T. Ohta, *IEEE International Conference on Nano/Micro Engineered and Molecular Systems (NEMS)*, 2014.
29. W. Hu, K. Ishii and A. Ohta, *2012 IEEE International Conference on Robotics and Automation (ICRA)*, 2012, 733-738.
30. P. Marmottant, J. P. Raven, H. Gardeniers, J. G. Bomer and S. Hilgenfeldt, *J Fluid Mech*, 2006, **568**, 109-118.
31. A. N. Hellman, K. R. Rau, H. H. Yoon and V. Venugopalan, *J Biophotonics*, 2008, **1**, 24-35.
32. W. Hu, Q. Fan and A. T. Ohta, *Lab Chip*, 2013, **13**, 2285-2291.
33. P. Prentice, A. Cuschierp, K. Dholakia, M. Prausnitz and P. Campbell, *Nat Phys*, 2005, **1**, 107-110.
34. Z. Fan, H. Liu, M. Mayer and C. X. Deng, *Proc Natl Acad Sci U S A*, 2012, **109**, 16486-16491.
35. R. P. Joshi and K. H. Schoenbach, *Physical Review E*, 2000, **62**, 1025-1033.
36. C. E. Pedraza, D. C. Bassett, M. D. McKee, V. Nelea, U. Gbureck and J. E. Barralet, *Biomaterials*, 2008, **29**, 3384-3392.
37. D. Hernandez, A. N. Melidoni, R. Phillips l and E. A. Shephard, *Methods Mol Biol*, 2006, **320**, 329-341.